INTERNATIONAL JOURNAL OF SATELLITE COMMUNICATIONS AND NETWORKING
Int. J. Satell. Commun. Network. 2018; **36**:44–65
Published online 8 December 2016 in Wiley Online Library (wileyonlinelibrary.com). DOI: 10.1002/sat.1203

Tri-orthogonal polarization diversity reception for non-geosynchronous satellite orbit ionospheric channels

Nicholas P. Lawrence[1,*,†], Hedley J. Hansen[1,2] and Derek Abbott[1]

[1]*School of Electrical and Electronic Engineering, The University of Adelaide, Adelaide, SA 5005, Australia*
[2]*RFT Group EWRD, DST Group Edinburgh, PO Box 1500, Edinburgh, SA 5111, Australia*

SUMMARY

Electromagnetic signals propagating through the ionosphere are subject to path delay and the depolarizing effect of Faraday rotation. These are both dependent on global position and link geometry, which constantly vary for satellites in non-geosynchronous orbits. These effects introduce performance error and reduce range resolution of remote sensing polarimetric measurements. Communication with ground receivers may be severely degraded by these effects. In this paper, a tri-orthogonal approach at the receiver is introduced to enhance performance of conventional polarization diverse receive schemes. Performance is measured through a capacity metric. The work presented forms part of a large-field-of-view, non-geosynchronous satellite model exploiting tri-orthogonal receive polarimetry as a means to enhancing link performance in a field-of-view. Copyright © 2016 John Wiley & Sons, Ltd.

Received 10 May 2016; Revised 12 October 2016; Accepted 9 November 2016

KEY WORDS: satellite; NGSO; LEO; Faraday rotation; path delay; polarization; channel capacity

1. INTRODUCTION

Many ground receive antennas relying on communication with non-geostationary satellites, including those used for voice and data communications, global telemetry, tracking, and command applications, and Global Positioning Systems (GPS), offer optimum performance through a maximized radiation gain pattern in a zenith direction. This performance degrades as the communication link between satellite and receiver moves away from this alignment. Moreover, as a means of avoiding communication degradation resulting from reduced power reception due to the depolarizing effect of Faraday rotation, satellite systems typically provide link reliability using circular polarization (CP) wave propagation. This form of polarization provides diversity and may be fundamentally resolved into two orthogonal linear polarized (LP) waves, with a $\pm 90°$phase offset between them [1]. This phase offset determines whether right-handed CP (RHCP), or left-handed CP wave propagation occurs. For an aligned system, CP propagation provides a higher probability of signal reception, after signal propagation through a depolarizing medium, than its LP counterpart. Wavemode propagation using CP and LP waveforms represents two extremes of the more general form of elliptical polarization (EP). The penalty for link reliability using CP propagation is that range may be reduced, as 3 dB of transmitted signal power is emitted from an orthogonal transmit polarization, or branch. The radiating surface of a CP patch antenna as a ground receiver is typically aligned with its radiating surface orthogonal to the zenith, providing optimal performance in the zenith direction [2, 3]. Coupled with a large gain reduction at low satellite angle elevations [4], polarization diversity at the receiver is degraded to little more than LP performance.

*Correspondence to: Nicholas P. Lawrence, School of Electrical and Electronic Engineering, The University of Adelaide, SA 5005, Australia.
† E-mail: nicholas.lawrence@adelaide.edu.au

With a ground receive antenna aligned for optimal zenith performance, a satellite passing overhead and transmitting a CP waveform in a sub-satellite, or nadir, direction transmits along the shortest possible channel link. At equatorial latitudes, ionospheric effects such as Faraday rotation and path delay on a propagating signal are typically weak in the nadir direction, due to both a short ionospheric path length and low interaction between the transmitted signal and the terrestrial magnetic field. As link geometry diverges from this aligned case, receive performance is typically more difficult to maintain as antenna misalignment increases, because of fundamental radiation pattern constraints of a CP antenna [5]. At higher latitudes, within the polar regions for example, an increased strength and inclination of the terrestrial magnetic field component [6] increases the possibility of degraded receiver performance [7]. This degradation may be further exacerbated by the possibility of a reduced satellite coverage according to a satellite application.

A satellite may transmit a CP waveform and thus provide polarization diversity, in a unique direction of propagation. At the receiver, angular departure from this direction of propagation causes reception to become EP, as a signal is received that does not demonstrate an axial ratio of 0 dB [8]. For a CP ground patch antenna receiver, orientated with radiating surface orthogonal to the zenith, reception in any off-zenith receive angle degrades polarization diversity. From a vectorial standpoint, this degradation becomes severe at the receiver horizon and may typically result in LP, or horizontally polarized, reception alone and an accompanying lack of polarization discrimination. Coupled with a reduced gain profile of the receive antenna for low receive elevation angles, and depolarizing ionospheric effects on a propagating signal which are typically strong at such elevations due to a maximized path length and strong interaction between the signal and a parallel component of the terrestrial magnetic field [9], link reliability can no longer be guaranteed over the extent of a satellite field-of-view (FoV). In this paper, we consider the FoV to be a circular area on the Earth seen from the perspective of the satellite in which a receive antenna may be positioned. The size of the FoV is determined by satellite orbit height, with the ground range at which the radiating surface of the receive antenna is orthogonal to an incoming satellite signal providing the circular FoV perimeter. Details of the FoV are expanded upon in Section 2. Furthermore, a lack of polarization diversity at the receiver may occur when optimal CP performance is expected: with a transmitting satellite at the zenith of a CP patch antenna on a boat, link performance may be compromised in rough sea conditions, for example, where severe receive antenna misalignment occurs as the boat travels up and down a wavefront.

The problem is prevalent for low-Earth-orbit (LEO) satellite systems, where relative link geometry varies rapidly as a function of time [10, 11]. To counter detrimental effects on a transmitted signal, a ground receiver may be perfectly aligned with a transmitting satellite, using manual or mechanical means, provided the location of the satellite is known. This may not always be possible and may be subject to mechanical failure.

Polarization diverse receive antennas, such as geodetic radomes and patch antennas, may receive signals from satellites in non-geosynchronous orbits and exhibit a low gain, and so low noise, optimal zenith performance with a large gain roll-off as departure is made from the zenith direction [4]. Cross-polarization rejection is degraded as the elevation of received signal decreases. Ideally, we would like to avoid the constraint of link geometry on antenna operation. In the case of global navigation satellite systems, receiving simultaneous signals from satellites provides a more accurate global position [12].

Synthetic aperture radar systems operating at L-band (1–2 GHz) use polarization diversity in the form of horizontally and vertically polarized waveforms as a means of mitigating Faraday rotation depolarization. In [13], a Faraday rotation of just 5° is suggested as reducing the dynamic range of wanted copolarized channels while driving cross-polarized channels to resemble copolarized channels. As a consequence, sensitivity is reduced to the point that differentation of received ground backscatter is severely degraded. In effect, when cross polarization rejection is degraded, the polarization diversity of a dual polarized antenna degrades towards that of a singularly polarized one.

Detrimental effects on LEO satellite communication receivers, typically operating at L-band frequencies and lower, may also increase due to suboptimal cross-polarization rejection at low elevation angles, as gain is optimized at the zenith and rolls off with decreasing elevation [14]. Specular reflections on a propagating signal, where 180° phase changes occur, may render RHCP transmission as

DOI: 10.1002/sat

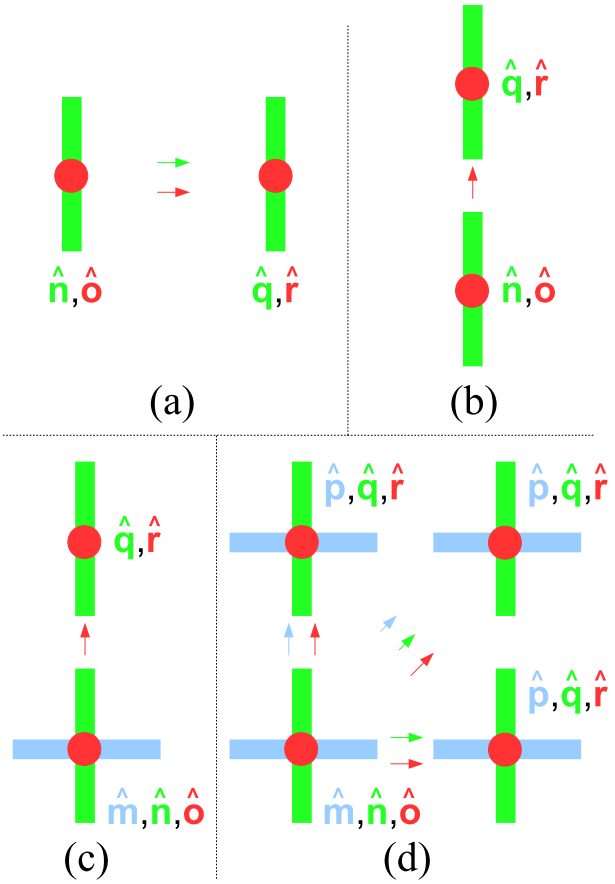

Figure 1. Tri-orthogonal arrangement: (a) full capacity is observed between R consisting of orthogonal polarizations $\hat{\mathbf{q}}$, $\hat{\mathbf{r}}$, and T consisting of orthogonal polarizations $\hat{\mathbf{n}}$, $\hat{\mathbf{o}}$, as a result of perfect alignment. Polarizations $\hat{\mathbf{o}}$ and $\hat{\mathbf{r}}$ are vertical so point upwards out of the paper; (b) half capacity is observed at R as only polarization $\hat{\mathbf{r}}$ is broadside to T; (c) polarization $\hat{\mathbf{m}}$ is introduced at T. Half capacity is once again observed as only polarization $\hat{\mathbf{r}}$ is broadside to T; (d) full capacity is restored through inclusion of polarization $\hat{\mathbf{p}}$ at R. At least two orthogonal polarizations are offered in any link direction. In this paper, polarization $\hat{\mathbf{o}}$ is omitted from T in order to accurately represent three *in situ* satellite system configurations. [Colour figure can be viewed at wileyonlinelibrary.com]

left-handed CP propagation, with no signal reception at a RHCP configured receive antenna. Multipath may create signal cancellation from certain directions at the receive antenna, as the result of scattering effects and diffusion in the channel. Both specular reflections and multipath effects typically reduce signal reception at the receiver. For system operation over channels with satellites already in orbit, the receiver configuration becomes important in offering the possibility of enhanced system performance through diversity at lower elevation angles. Polarization purity in three orthogonal directions may improve reception at lower elevation angles and so extend the range of useful reception.

The advantages of polarization diversity through a tri-orthogonal antenna configuration have been presented in previous work, typically in consideration of terrestrial applications [15], but also over satellite channels [16]. Polarization diversity offers an alternative to satellite diversity that may suffer from synchronization effects, which are exacerbated for LEO satellites. Such a configuration offers an additional degree of freedom at the antenna over conventional CP techniques that may mitigate performance degradation due to ionospheric effects. The concept of a tri-orthogonal arrangement is illustrated in Figure 1. Over a satellite channel, ionospheric effects are both time and location dependent, and so to mitigate their effect over an entire FoV requires a generic solution. In this paper, tri-orthogonal polarization at the receiver is considered as a means to improving link performance.

DOI: 10.1002/sat

Table I. System information is provided below on three distinct satellite systems considered in this paper.

Type	Orbit (km)	Inclination (°)	Transmit Power (dBm)	Frequency (MHz)	Bandwidth (kHz)	Polarization	Gain $_{(T,boresight)}$ (dBic)	Gain$_{(R,max)}$ (dBic)
Iridium	780	86.4	27.7	1616	41.7	RHCP	23.1	3.7
Orbcomm	775	48.6	39	138	25	RHCP	0.8	4.5
GPS	20200	55	25.4	1575 (L1)	2000	RHCP	13.1	3.7

2. METHOD

Three distinct non-geosynchronous satellite systems are analyzed, all transmitting an RHCP signal; the LEO Iridium satellite system [17, 18], the LEO Orbcomm Telemetry, Tracking, and Command (TT&C) system [19, 20] and the GPS system [21], operating in a mid-Earth-orbit.

A novel vectorized model is described using a fundamental physical approach, which uses real-time ionospheric data inputs, in order to calculate system channel capacity at the receiver for system operation with and without a third orthogonal polarization at the receiver. Constant transmit power is assumed in these calculations.

The characteristics of the three satellite systems are given in Table I. The transmitter at the satellite shall be referred to as T, with the receiver on the ground referred to as R. The gain at T is denoted as G_{T}. The gain at R is denoted as G_{R}. We assume the ground receiver at R to be planar in nature, with a volume of a conventional CP patch antenna.

2.1. Link geometry

The link geometry is given according to [10] and is illustrated in Figure 2. An Earth-centered Earth-fixed (ECEF) coordinate system is invoked for this work. The x-axis is positioned at the latitude, longitude position (0,0). In a first instance, we may generate the FoV about this axis. At the FoV center, an easterly direction $[010]^T$, where the superscript refers to transpose, coincides with an azimuthal angle θ_T of 0°. Within the FoV, anti-clockwise rotation is deemed as positive. Figure 3 demonstrates the concept, with the five system polarizations labelled as $\hat{\mathbf{m}}$ to $\hat{\mathbf{r}}$. These will be determined in vector form in Section 2.2. Link geometry is determined according to the following equations:

$$\gamma = \frac{r_{\mathrm{plot}}}{r_{\mathrm{e}}} \tag{1}$$

$$s = \sqrt{u^2 + r_{\mathrm{e}}^2 - 2u r_{\mathrm{e}} \cos\gamma} \tag{2}$$

$$\kappa = \arcsin\left(\frac{u}{s}\sin\gamma\right) \tag{3}$$

$$\alpha = \arcsin\left(\frac{u}{s}\sin\gamma\right) - \gamma \tag{4}$$

$$\gamma_{max} = \arccos\left(\frac{r_{\mathrm{e}}}{u}\right) \tag{5}$$

$$s_{max} = \sqrt{u^2 - r_{\mathrm{e}}^2} \tag{6}$$

$$\alpha_{max} = \arcsin\left(\frac{r_{\mathrm{e}}}{u}\right) \tag{7}$$

DOI: 10.1002/sat

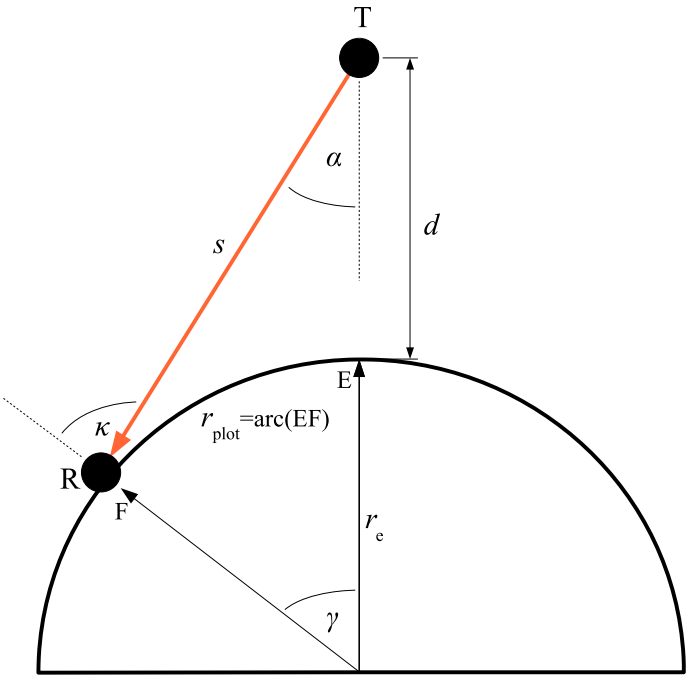

Figure 2. Link geometry: Transmitter T is in an orbit of height d. The receiver R is positioned on a semi-circle determined by simple trigonometry. Propagation from T to R is along the path of length, s. At any FoV position, the radial distance from the FoV center is a function of angle α or angle γ together with the radius of the Earth. The entire system is rotated about the FoV center by 360° to develop a spherical surface. The number of concentric paths on the sphere together with the azimuthal step increment about the FoV center is set by the user. The simulation begins at the FoV center and works outward to the concentric circle where $\kappa = 90°$. [Colour figure can be viewed at wileyonlinelibrary.com]

where r_e is the 6378 km radius of the Earth and u is $r_e + d$, d being orbit height. A link unit vector $\hat{\mathbf{k}}$ from T to R is determined for all positions in the FoV by

$$\hat{\mathbf{k}} = \begin{bmatrix} -\cos\alpha \\ \cos\theta_T \sin\alpha \\ \sin\theta_T \sin\alpha \end{bmatrix}. \tag{8}$$

The perimeter of the FoV is determined as the ground range at which $\kappa = 90°$, as seen in Figures 2 and 3. Elevation at T is given by α with 0° in the nadir direction, otherwise positive. Elevation at R is given by κ with 0° in the zenith direction, otherwise positive. The azimuthal angle θ_R at R of the vector representing signal propagation $\mathbf{k}$ differs to that of the corresponding angle θ_T at T by 180°. The receiver R is assumed to be at a distance s from T that changes according to FoV location. The FoV may subsequently be positioned, according to its center, at any user specified (L_u, l_u) global position.

2.2. *Transmitter and receiver arrangement*

In Figure 3, we position orthogonal polarizations $\hat{\mathbf{m}}$, $\hat{\mathbf{n}}$, representing CP wave transmission, that are respectively aligned in an easterly and northerly direction at (L_o, l_o), or (0,0).

To increase system performance over a large-FoV, polarization diversity using a tri-orthogonally polarized structure is employed at R. Polarizations $\hat{\mathbf{p}}$, $\hat{\mathbf{q}}$, and $\hat{\mathbf{r}}$ are respectively aligned in an easterly, northerly, and radial direction. The radial polarization, $\hat{\mathbf{r}}$, at R becomes increasingly broadside to transmission from T as movement is made to the outer edge of the FoV. At the outer edge of the FoV, it becomes fully broadside, offering optimal alignment and gain characteristics, and the possibility of dual polarization as the performance of either $\hat{\mathbf{p}}$ or $\hat{\mathbf{q}}$ degrades. We assume R to be stationary, that is to say, with no vector displacement. In this analysis, we maintain a 3×3 channel matrix for ease of matrix manipulation by inclusion of a third orthogonal polarization $\hat{\mathbf{o}}$ at T. Once the final channel

DOI: 10.1002/sat

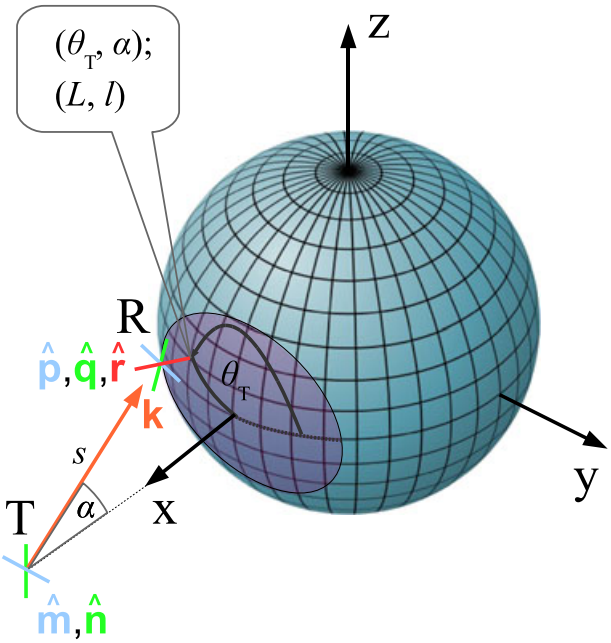

Figure 3. System according to specific location in field-of-view. An Earth-centered Earth-fixed coordinate system locates position in three-dimensional space. Propagation is from T, using two orthogonal polarizations to represent circular polarization wave transmission, to the tri-orthogonal arrangement at R along a path of length s. The five system polarizations are labelled $\hat{\mathbf{m}}$ to $\hat{\mathbf{r}}$. Link direction is given by a propagation vector, $\mathbf{k}$. Propagation to a point in the FoV is determined by α and θ_T. These angles correspond to a (latitude, longitude), or (L, l), global position enabling link characteristics to be determined as a function of global location and FoV geometry. [Colour figure can be viewed at wileyonlinelibrary.com]

matrix is calculated, of 3×3 form, capacity is calculated according to transmission from polarizations $\hat{\mathbf{m}}$ and $\hat{\mathbf{n}}$, or the left hand and middle column of the matrix only. Any CP signal transmission in a direction, in this paper from three *insitu* satellites at T, may be fundamentally described using an arrangement of two linear collocated orthogonally polarized transmitted waveforms, in this case with polarizations $\hat{\mathbf{m}}$ and $\hat{\mathbf{n}}$, a relative phase difference of 90°, and a superimposed gain pattern or directivity in the direction of transmission, including a third orthogonal polarization at R effectively provides two orthogonal reception polarizations for signal reception from any link direction.

We may describe five polarization orientations according to their latitude (L) and longitude (l) positions within the FoV. At T, we have

$$\hat{\mathbf{m}} = \begin{bmatrix} -\sin l_{\mathrm{o}} \\ \cos l_{\mathrm{o}} \\ 0 \end{bmatrix} \tag{9}$$

$$\hat{\mathbf{n}} = \begin{bmatrix} -\sin L_{\mathrm{o}} \cos l_{\mathrm{o}} \\ -\sin L_{\mathrm{o}} \sin l_{\mathrm{o}} \\ \cos L_{\mathrm{o}} \end{bmatrix}. \tag{10}$$

At R, we have

$$\hat{\mathbf{p}} = \begin{bmatrix} -\sin l \\ \cos l \\ 0 \end{bmatrix} \tag{11}$$

$$\hat{\mathbf{q}} = \begin{bmatrix} -\sin L \cos l \\ -\sin L \sin l \\ \cos L \end{bmatrix} \tag{12}$$

DOI: 10.1002/sat

$$\hat{\mathbf{r}} = \begin{bmatrix} \cos L \cos l \\ \cos L \sin l \\ \sin L \end{bmatrix}. \tag{13}$$

For completeness, we introduce the third polarization $\hat{\mathbf{o}}$, orthogonal to $\hat{\mathbf{m}}$ and $\hat{\mathbf{n}}$, at T as,

$$\hat{\mathbf{o}} = \begin{bmatrix} \cos L_o \cos l_o \\ \cos L_o \sin l_o \\ \sin L_o \end{bmatrix}. \tag{14}$$

Latitude and longitude (L,l) determination is given in the next section.

2.3. Latitude and longitude determination

We begin by determining a FoV center (L_c, l_c), along an orbit track and according to orbit parameters, and the user specified FoV center starting point, (L_o, l_o), which we set at (0°,0°) for ease of understanding. After a time t, and with the satellite orbit dictating a tangential velocity of $\mathbf{v}_T$, of magnitude given by Kepler orbital mechanics, and of direction given by an orbital inclination angle, θ_{inc}, where this angle is positive for counter clockwise rotation about the x-axis and is 0°for an easterly direction, we arrive at the new FoV center, (L_c, l_c). A unique satellite bearing angle at (L_o, l_o), which is 0° in a northerly direction and positive for a clockwise rotation about the x-axis, is determined as,

$$\theta_{bFoV} = \left| 2.5\pi - \theta_{inc}, 2\pi \right| \tag{15}$$

where θ_{inc} values for all three satellites are given in Table I.

All (L, l) positions of R within a second FoV centered at (L_c, l_c), required for determination of ionospheric parameters of total electron content (TEC), and terrestrial magnetic field vector, or $\mathbf{b}$, are determined from the FoV center latitude and longitude, (L_c, l_c), given respectively from (L_o, l_o) and θ_{bFoV} as,

$$\begin{aligned} L_c = \arcsin\{&\sin(L_o)\cos(\|\mathbf{v}_T\|t/u) \\ &+ \cos(L_o)\sin(\|\mathbf{v}_T\|t/u)\cos\theta_{bFoV}\} \end{aligned} \tag{16}$$

$$\begin{aligned} l_c = l_o - \frac{2\pi t}{86400} + \text{atan}_2\{&\sin\theta_{bFoV}\sin(\|\mathbf{v}_T\|t/u)\cos(L_o), \\ &\cos(\|\mathbf{v}_T\|t/u)\sin(L_o)\sin(L_c)\} \end{aligned} \tag{17}$$

where the function $\text{atan}_2\,(a, b)$ is given as

$$\text{atan}_2(a,b) = \begin{cases} \arctan(\frac{a}{b}) & (b \succ 0) \\ \arctan(\frac{a}{b}) + \pi & (a \succeq 0, b \prec 0) \\ \arctan(\frac{a}{b}) - \pi & (a \prec 0, b \prec 0) \\ +\pi/2 & (a \succ 0, b = 0) \\ -\pi/2 & (a \prec 0, b = 0) \\ \text{undefined} & (a = 0, b = 0) \end{cases}. \tag{18}$$

We proceed to calculate latitude and longitude, or (L, l), positions for every position within the FoV. The number of positions within the FoV are user defined through increments of the azimuthal and off-nadir angles, θ_T, and α, respectively. Global positioning through (L, l) doublets for each of these positions may be given by the following formulae [22], the FoV being centered at (L_c, l_c),

$$\begin{aligned} L = \arcsin\{&\sin(L_c)\cos(r_{plot}/r_e) \\ &+ \cos(L_c)\sin(r_{plot}/r_e)\cos\theta_b\} \end{aligned} \tag{19}$$

DOI: 10.1002/sat

$$l = l_c + \text{atan}_2\{\sin\theta_b \sin(r_{plot}/r_e)\cos(L_c), \cos(r_{plot}/r_e)\sin(L_c \sin(L)\} \tag{20}$$

where θ_b is a bearing angle from the FoV center (L_c, l_c) to a (L, l) position in the FoV and is related to θ_T by

$$\theta_b = \left| 2.5\pi - \theta_T, 2\pi \right|. \tag{21}$$

We aim to perform vector calculation within the FoV centered at (L_o, l_o). The unit vectors $\hat{\mathbf{m}}$, $\hat{\mathbf{n}}$, and $\hat{\mathbf{r}}$ do not vary as a function of FoV center, although $\hat{\mathbf{r}}$ does change over the FoV. The orientation of polarization unit vectors $\hat{\mathbf{p}}$ and $\hat{\mathbf{q}}$ is given by (11) and (12), respectively, following determination of (L, l) values obtained from (19) and (20). They may be rotated into the FoV centered at (L_o, l_o) according to

$$\hat{\mathbf{p}}_{\text{FoV(Lo,lo)}} = \mathbf{R}_{-l}\mathbf{R}_{-L}\hat{\mathbf{p}}_{\text{FoV(Lc,lc)}} \tag{22}$$

and

$$\hat{\mathbf{q}}_{\text{FoV(Lo,lo)}} = \mathbf{R}_{-l}\mathbf{R}_{-L}\hat{\mathbf{q}}_{\text{FoV(Lc,lc)}} \tag{23}$$

where

$$\mathbf{R}_L = \begin{bmatrix} \cos(L) & 0 & -\sin(L) \\ 0 & 1 & 0 \\ \sin(L) & 0 & \cos(L) \end{bmatrix} \tag{24}$$

and

$$\mathbf{R}_l = \begin{bmatrix} \cos(l) & -\sin(l) & 0 \\ \sin(l) & \cos(l) & 0 \\ 0 & 0 & 1 \end{bmatrix}. \tag{25}$$

The (L, l) values obtained from (19) and (20) allow for determination of the ionospheric parameters of TEC, and terrestrial magnetic field vector, $\mathbf{b}$. They may subsequently be introduced into the analgous FoV centered at (L_o, l_o) for subsequent vector calculation.

2.4. The channel

A satellite channel does not typically provide a rich scattering environment that may benefit signal propagation in, for example, a densely populated urban environment employing wireless frequencies typically less than 6 GHz. Satellite channels are typically low rank and line-of-sight (LoS) [23, 24]. A complex Ricean fading channel matrix $\mathbf{H}$ may be decomposed into the sum of an average LoS component ($\bar{\mathbf{H}}$) and a variable scattered NLoS component ($\tilde{\mathbf{H}}$) given by

$$\mathbf{H} = \sqrt{\frac{K}{1+K}}\bar{\mathbf{H}} + \sqrt{\frac{1}{1+K}}\tilde{\mathbf{H}} \tag{26}$$

where K is the Ricean K-factor that determines the proportion of LoS and NLoS signal components arriving at R, after signal propagation through the channel. In this manuscript, a pure LoS channel shall be assumed for the Orbcomm and GPS systems, as this forms the basis on which statistical interpretation of channel fading may be applied. As such, the NLoS component, $\tilde{\mathbf{H}}$, is omitted for these two satellite systems. For the Iridium system, local scattering effects shall be included, and as such, we shall include a NLoS component. For the system shown in Figure 3, the channel has six subchannels as we consider $insitu$ CP transmission from T. These are the first two columns of the 3×3 channel matrix in (27) that includes subchannels arising from transmission of a third orthogonal polarization $\hat{\mathbf{o}}$ at T. The channel, which is of rank 2, may be given as

DOI: 10.1002/sat

$$\mathbf{H} = \begin{bmatrix} h_{\hat{\mathbf{p}}\hat{\mathbf{m}}} & h_{\hat{\mathbf{p}}\hat{\mathbf{n}}} & h_{\hat{\mathbf{p}}\hat{\mathbf{o}}} \\ h_{\hat{\mathbf{q}}\hat{\mathbf{m}}} & h_{\hat{\mathbf{q}}\hat{\mathbf{n}}} & h_{\hat{\mathbf{q}}\hat{\mathbf{o}}} \\ h_{\hat{\mathbf{r}}\hat{\mathbf{m}}} & h_{\hat{\mathbf{r}}\hat{\mathbf{n}}} & h_{\hat{\mathbf{r}}\hat{\mathbf{o}}} \end{bmatrix} \tag{27}$$

where the matrix coefficients represent signal transfer between a polarization pair. The channel $\mathbf{H}$ is calculated for all (L, l) positions within the FoV.

Several factors affect signal transfer between the six polarization pairs, and the Friis transmission equation is used to describe these. For a polarization pair such as $\hat{\mathbf{r}}\hat{\mathbf{m}}$, the polarization mismatch may be given by the inner product in (28) [25],

$$e_{\mathrm{pol}(\hat{\mathbf{r}}\hat{\mathbf{m}})} = |\hat{\mathbf{r}}_{\perp\mathbf{k}} \cdot \hat{\mathbf{m}}_{\perp\mathbf{k}}|^2 \tag{28}$$

where $\hat{\mathbf{r}}_{\perp\mathbf{k}}$ and $\hat{\mathbf{m}}_{\perp\mathbf{k}}$ are projections onto the plane perpendicular to the unit propagation vector $\hat{\mathbf{k}}$.

The projection of an arbitrary vector $\mathbf{v}$ onto the plane perpendicular to $\hat{\mathbf{k}}$ may be given by

$$\mathbf{v}_{\perp\mathbf{k}} = \left(\mathbf{I_3} - \hat{\mathbf{k}}\hat{\mathbf{k}}^{\mathrm{T}}\right)\hat{\mathbf{v}}, \tag{29}$$

which may be normalized to give

$$\hat{\mathbf{v}}_{\perp\mathbf{k}} = \frac{\mathbf{v}_{\perp\mathbf{k}}}{|\mathbf{v}_{\perp\mathbf{k}}|}. \tag{30}$$

Boresight gains for waveforms at T and maximum gains for received waveforms at R are introduced in Table I.

Considering the Orbcomm system, for the gain profiles of waveforms transmitted with polarizations $\hat{\mathbf{m}}$ and $\hat{\mathbf{n}}$ at T, we place a shaped profile according to [26], where a 0.8 dBic gain is observed at broadside, or α=0°, which increases to a maximum of 3.7 dBic at 55°off-nadir, or $\alpha = 55°$. For the Iridium and GPS systems, we introduce ideal conical beam gain profiles at T which compensate additional free space path loss for non-nadir path propagation [27, 28]. Transmit frequencies for the Iridium and GPS L1 systems are close together, straddling 1.6 GHz, and as such, receive antennas are typically packaged to cater for both as a patch-style unit [4]. Receive antennas for the Orbcomm system provide a similar low-gain radiation pattern. We note that patch-style and vertical whip antennas are commercially available [29, 30], and opt for a patch-style antenna in our simulation, so that RHCP reception may be considered. We introduce the power gain of a half-wavelength dipole, G, [25], and assume 100% dipole efficiency. Minimum gain occurs when elevation ϕ is 0°, or at the endfire position. Maximum gain occurs when ϕ is 90°, or at the broadside position, and is independent of the azimuthal angle, θ. For all three satellite systems, we note the similarity in low-gain profiles at R in Table I. These antennas are designed for a wide hemispherical angle of reception and low noise. In this paper, we base the gains associated with polarizations $\hat{\mathbf{p}}$ and $\hat{\mathbf{q}}$ at R on that of a half-wavelength dipole, which is a realistic approximation of a typical low gain CP receive antenna. In addition, we introduce polarization $\hat{\mathbf{r}}$, orthogonal to polarizations $\hat{\mathbf{p}}$ and $\hat{\mathbf{q}}$, and also exhibiting a half-wavelength dipole power gain. As polarizations $\hat{\mathbf{p}}$ and $\hat{\mathbf{q}}$ are common to both a CP receive antenna and a tri-orthogonal arrangement, so any improvement in receive performance is purely as a result of the inclusion of polarization $\hat{\mathbf{r}}$ at R. We maintain symmetry of the CP radiation pattern at R after inclusion of polarization $\hat{\mathbf{r}}$ through a phase centered approach that employs a sequential feeding technique [31].

In the case of polarization $\hat{\mathbf{r}}$ at R, angle ϕ is represented by κ, the sum of α and γ, as in Figure 2. It is important to recognize that the gain profile, as well as the polarization mismatch profile, changes for $\hat{\mathbf{p}}$ and $\hat{\mathbf{q}}$ at R as a function of latitude and longitude within the FoV. For polarizations $\hat{\mathbf{p}}$ and $\hat{\mathbf{q}}$, we use the following equation,

$$G(\theta, \phi) = 1.64|\hat{\mathbf{v}} \wedge \hat{\mathbf{k}}|^3 \tag{31}$$

where $\hat{\mathbf{v}}$ represents the unit vector of the polarization in question.

DOI: 10.1002/sat

2.5. Faraday rotation and path delay

Faraday rotation and path delay are considered to be the two principal effects that affect signal propagation through the ionosphere [32]. These effects may be determined through link geometry, together with TEC data and terrestrial magnetic field data. TEC data are available in 10 min intervals [33], while terrestrial magnetic field data are available on a daily time scale [6]. Values of TEC typically range from 1 to 100, for a vertical path through the ionosphere. Magnetic field ranges are readily interrogated within the World Magnetic Model supplied in the MATLAB environment.

Height h along the propagation path from T to R is determined as

$$\begin{aligned} h = {} & (r_{\mathrm{e}} + d) \\ & - \left\{ \left\{ r_{\mathrm{e}} \{1 - \cos \gamma_{\mathrm{i_{FR}}}\} + d \right\} \times \frac{d(k_{\mathrm{FR}} - 1)}{(i_{\mathrm{FR}} - 1)} \right\} \\ & - r_{\mathrm{e}} \cos \gamma_{\mathrm{k_{FR}}}. \end{aligned} \tag{32}$$

In (32), i_{FR} is the ith incremental position in terms of α from the nadir, and k_{FR} is a variable running from the nadir position along a constant azimuthal path, θ_{T}, to the ith incremental position of α. Figure 5 illustrates the concept. Propagation to an FoV (L, l) doublet position is along a path with a constant azimuthal angle, θ_{T}.

The simulation computes the propagation vector, $\hat{\mathbf{k}}$, and all investigated effects starting at the FoV center or nadir position at $\theta_{\mathrm{T}} = 0$. The simulation refers to each FoV position in turn through increments of θ_{T} that, after completion of one circle, moves radially outward by an increment of the off-nadir angle, α.

Considering transmission to a receiver position, R1, with regard to ionospheric effects, the introduction of h creates (L, l, h) triplets where h is calculated at each (L, l) doublet position along a unique path, given by $\hat{\mathbf{k}}_{\mathrm{R1}}$, to the receiver position, $(L_{\mathrm{R1}}, l_{\mathrm{R1}})$. Once the accompanying effects of Faraday rotation and path delay have been computed for propagation from T to R1, the simulation moves to position R2. New values of h must be assigned to each (L, l) position along a propagation path each time a new receiver position is considered. Receiver positions on the same concentric circle utilize the same values of h along the path.

The values of h are used in the determination of the Earth's magnetic field vector. Along a propagation path from T to R, globally referenced positions are passed through at progressively reduced heights with each set of encountered (L, l, h) triplets subsequently introducing an accompanying set of magnetic field vector and TEC data. These data are then used to generate estimates of Faraday rotation and path delay [34]. These estimates are based on the following trigonometric equations [35] but differ from them as a result of tapping ionospheric data at mutiple points along the propagation path, providing vectorized estimates at the receiver.

Faraday rotation and path delay are respectively given as

$$\psi_{\mathrm{FR}} = \frac{e^3 \lambda^2}{8\pi\epsilon_0 m^2 c^3} \int_0^s n_{\mathrm{e}}(s) \mathbf{b}_{||}(s) ds \tag{33}$$

and

$$\zeta = K_{\mathrm{ref}} \frac{\mathrm{TEC}}{f^2 \cos \alpha} \tag{34}$$

where s is propagation path length, $\mathbf{b}_{||}$ is the component of the terrestrial magnetic field parallel to signal propagation, e is electronic charge, λ is propagating signal wavelength, ϵ_0 is the permittivity of free space, m is electronic mass, c is the speed of light *in vacuo*, K_{ref} is a dimensionless constant of ionospheric refraction set at 40.28 [35], TEC is the TEC along the propagation path, f is the signal frequency and α is an off-nadir angle that is used to account for the additional path length of a slanted path. Determination of the Earth's magnetic field vector at a triplet position is according to [6]. Each terrestrial magnetic field unit vector may be orientated into the ECEF coordinate system beginning

DOI: 10.1002/sat

with an ECEF northerly pointing unit vector, $\hat{\mathbf{n}}$ or $[001]^{\mathrm{T}}$, at (0°,0°). This is rotated by the declination, δ, and inclination, ι, of the magnetic field vector for a given height,

$$\mathbf{R}_{\delta} = \begin{bmatrix} 1 & 0 & 0 \\ 0 & \cos\delta & -\sin\delta \\ 0 & 0 & 1 \end{bmatrix} \tag{35}$$

$$\mathbf{R}_{\iota} = \begin{bmatrix} \cos\iota & 0 & \sin\iota \\ 0 & 1 & 0 \\ -\sin\iota & 0 & \cos\iota \end{bmatrix}. \tag{36}$$

Convention gives δ as positive in an easterly direction and ι as positive in a downward direction. The magnetic field unit vector may then be rotated to the appropriate (L, l) position in the FoV centered at $(L_{\mathrm{o}}, l_{\mathrm{o}})$,

$$\hat{\mathbf{b}}_{\mathrm{L,l,h}} = \mathbf{R}_{\mathrm{L}}\mathbf{R}_{\mathrm{l}}\mathbf{R}_{\delta}\mathbf{R}_{\iota}\hat{\mathbf{n}}_{0,0} \tag{37}$$

where the rotation matrices, $\mathbf{R}_L$ and $\mathbf{R}_l$, are as per (24) and (25). Magntitudes given by [6] are attributed to each triplet (L, l, h) position.

Determination of the TEC value at a (L, l) position is given by [33]. Values of TEC in this paper are from 1 to 100. The data are coarse with resolution of (2°,18°). In order to produce a smooth interpretation of TEC for each (L, l) doublet in the FoV, bilinear interpolation is invoked. This is pertinent as most (L, l) positions do not align with the global positions used in the data collection performed in [33].

The TEC for a (L, l) nadir path is determined by the multiplication of a TEC value given by [33] with a TECU or TEC unit defined globally as 10^{16} electrons per m^2 [35]. The resultant path value, VTEC, refers to the number of free electrons in a vertical column of cross section 1 m^2 along the nadir path at a specified (L, l) position and may be given as

$$\mathrm{VTEC} = \int_{s_{(\mathrm{nadir})}} n_{\mathrm{e}} ds_{(\mathrm{nadir})} \tag{38}$$

where n_{e} refers to the electron density along the nadir path, s_{nadir} [36].

Variability of interaction between ionized particles and an electromagnetic signal propagating along a path between transmitter and receiver is accounted for by the introduction of an interaction length over which the magnetic field vector and TEC, respectively, (L, l, h) and (L, l) specific, interact with the signal. In Figure 5, s is assumed to be 1500 km. The FoV position is at the end of a constant azimuthal or θ_T trajectory path, at a position specified by α. For simplicity, it shall be known as α_3.

Three interaction lengths, shown with parametric subscripts, are delineated in Figure 5. Each length is 500 km and attributed to each of the three (L, l) doublet positions along the path. Over an interaction length, the TEC is given according to the accompanying (L, l) position. Magnetic field vector data are obtained using a (L, l, h) triplet position. A scaling factor is introduced to account for ionospheric electron density, as a function of height, along the propagation length [34]. It is noteworthy to observe that, as a result, the TEC becomes (L, l, h) specific for path effect calculations. The scaling factor is enhanced for this model to provide a two state diurnal ionosphere as a function of (l) and Coordinated Universal Time, or UTC. The two states are calculated as the mean of solar maxima and minima ionospheric electron density profiles for both day and night. The variation between day and night profiles stems from changes in ionospheric electron density at a specific altitude as a function of solar activity. In effect, the two diurnal states scale the interaction between the ionosphere and a propagating signal as a function of ionospheric electron density at a (L, l, h) position along a propagation path normalized by an average of ionospheric electron density in a vertical column that passes through the ionosphere at this (L, l, h) position. We assume the ionosphere to lie between 50 and 1000 km in geodetic altitude. Figure 4 shows the day and night scaling factors as a function of altitude. The scaling factors for both averaged day and night profiles provide a profile equivalent to a unity scale for propagation through the entire ionosphere. For off-nadir transmission, TEC may vary as a

DOI: 10.1002/sat

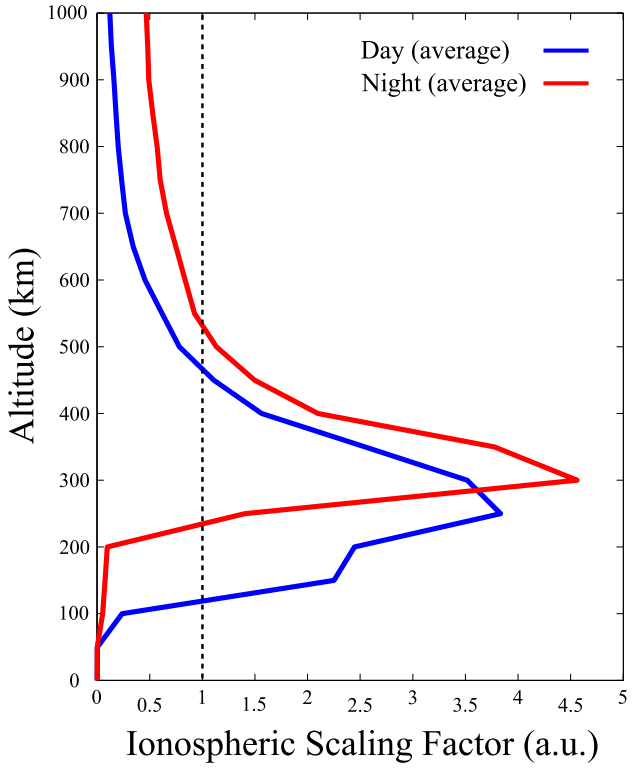

Figure 4. Two state or diurnal ionospheric scaling factors are averaged from solar maxima and minima profiles to make day and night averaged ionospheric profiles. Both of these profiles provide a profile equivalent to a unity scale for propagation through the entire ionosphere. For off-nadir transmission, total electron content may vary as a function of (L, l) position. By introducing the scaling factors, we provide the possibility of simulating ionospheric effects on a transmitted signal as a function of (L, l, h) position. [Colour figure can be viewed at wileyonlinelibrary.com]

function of (L, l) position. By introducing the scaling factors, we provide the possibility of simulating ionospheric effects on a transmitted signal as a function of (L, l, h) position. The Earth's rotation provides movement of longitudinal position at the angular rate of 15°/h, regardless of latitudinal position. As well as affecting the orbital position of a satellite, this movement affects the position of a ground receiver relative to the Sun. Coordinated Universal Time provides a reference that we may use in order to provide either of the two ionopsheric profiles in Figure 4.

Over each interaction length along the propagation path, values of magnetic field and TEC associated with each respective (L, l, h) triplet and (L, l) doublet are then used in (33) and (34). The resulting values from all interaction lengths are then integrated to provide an estimation of Faraday rotation and path delay for each (L, l) FoV position. Movement radially outward to the next concentric circle through increment of α redefines the parameters. In the case of Figure 5, the path is now split into four interaction lengths.

Faraday rotation is implemented in the simulation by a rotation of the polarizations $\hat{\mathbf{m}}$ and $\hat{\mathbf{n}}$, at T, about the propagation vector $\hat{\mathbf{k}}$, by the Faraday rotation angle. The effect of Faraday rotation is to improve subchannel propagation at some global locations while worsening it for others.

2.6. *Doppler frequency shift*

The direction of tangential velocity associated with T changes as a function of time, in order to maintain the orbit path, and is given by a shortest route bearing angle, θ_{sb},

$$\theta_{\mathrm{sb}} = \Big|\mathrm{atan}_2\{\sin(L_{\mathrm{o}} - L_{\mathrm{c}})\cos(L_{\mathrm{c}}), \cos(L_{\mathrm{c}})\sin(L_{\mathrm{o}}) - \sin(L_{\mathrm{c}})\cos(L_{\mathrm{o}})\cos(l_{\mathrm{o}} - l_{\mathrm{c}})\}, 2\pi\Big|. \tag{39}$$

DOI: 10.1002/sat

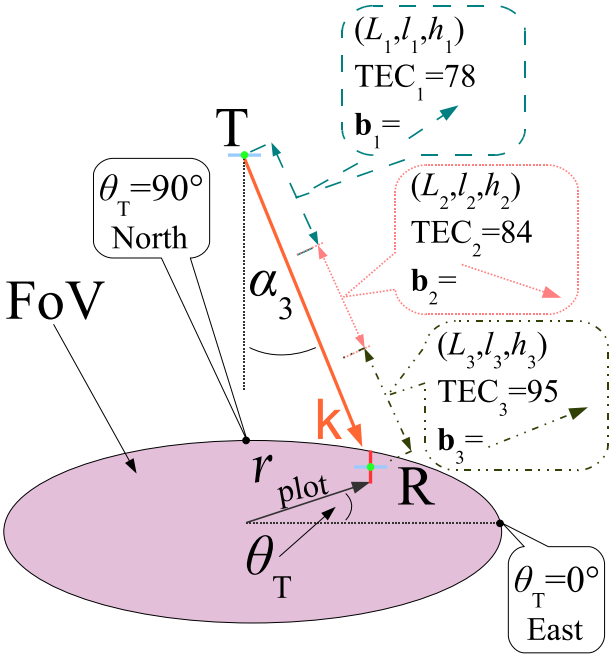

Figure 5. Height is calculated at each field-of-view (FoV) position along the propagation path. Each of these FoV positions has an accompanying (L, l) reference so forming a unique (L, l, h) triplet along a propagation path of length, s, and of direction given by the unit propagation vector, $\hat{\mathbf{k}}$. Associated magnetic field and TEC data are respectively attached to each triplet along the path. Interactions between the ionosphere and the propagation vector $\mathbf{k}$ along the path at each encountered FoV position are then integrated to provide an estimate of Faraday rotation and path delay, both specific to a (L, l) FoV position. This is repeated for all (L, l) FoV positions. [Colour figure can be viewed at wileyonlinelibrary.com]

Figure 6 illustrates the changing nature of the unit velocity vector, $\hat{\mathbf{v}}_T$, associated with T, as a function of global (L_c, l_c) position. In effect, the velocity vector of T, $\mathbf{v}_T$, is seen to rotate about the FoV center to $\mathbf{v}_{T'}$, as a function of global (L_c, l_c) position.

To determine the Doppler frequency shift as a function of the position of T along the orbit path, we start with the initial bearing angle at the center of the (L_o, l_o) FoV, θ_{bFoV}, and determine the bearing angle at the center of the (L_c, l_c) FoV, $\theta_{bFoV'}$. This is given as

$$\theta_{bFoV'} = \begin{cases} \theta_{sb} & (t = 0) \\ \theta_{sb} + \pi & \left(\left| \|\mathbf{v}_T\| t / r_e, 1 \right| \prec 0.5 \right) \\ \theta_{sb} & \left(\left| \|\mathbf{v}_T\| t / r_e, 1 \right| \succeq 0.5 \right). \end{cases} \tag{40}$$

We then align the (L_c, l_c) FoV with the initial (L_o, l_o) FoV on the x-axis, as illustrated in Figure 6. The bearing angle, $\theta_{bFoV'}$, may then rotate in the yz plane about the x-axis, as a function of FoV center position, (L_c, l_c), along the orbit path.

In the (L_c, l_c) FoV, the orbital inclination angle $\theta_{inc'}$ is analgous to that of the initial (L_o, l_o) FoV, θ_{inc}. It is used in conjunction with $\theta_{bFoV'}$, for the determination of the Doppler frequency shift uniquely, as a function of (L_c, l_c) FoV position,

$$\theta_{inc'} = \left| \theta_{bFoV'} - 2.5\pi, 2\pi \right|. \tag{41}$$

The tangential velocity unit vector of T for any FoV center position, (L_c, l_c), along the orbit path may be given as

$$\hat{\mathbf{v}}_T = \begin{bmatrix} 0 \\ \cos\theta_{inc'} \\ \sin\theta_{inc'} \end{bmatrix}. \tag{42}$$

DOI: 10.1002/sat

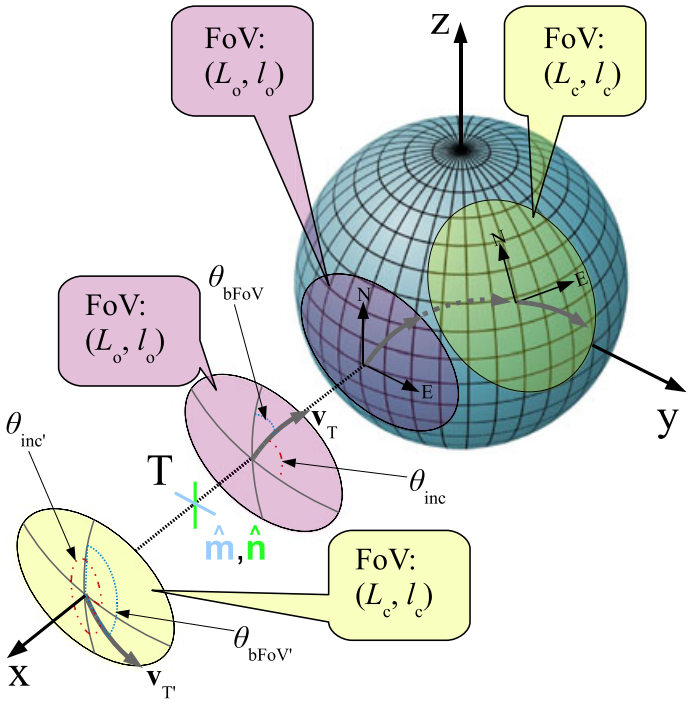

Figure 6. To maintain a trajectory along an orbit path, the velocity must change as a function of (L, l). This is calculated at each FoV center, at the (L_c, l_c) position of T. This allows calculation of the Doppler frequency shift, which for a low-Earth-orbit satellite channel is typically of the order of 30 kHz for a stationary ground receiver. [Colour figure can be viewed at wileyonlinelibrary.com]

For a LEO satellite orbiting at 780 km, the magnitude of tangential velocity is 7.470 kms^{-1}. If required, the ground velocity of R, $\mathbf{v}_R$, may be given according to a user defined magnitude and a unit vector direction $\hat{\mathbf{v}}_R$, specified by rotating $\hat{\mathbf{p}}$ around $\hat{\mathbf{r}}$ by a user defined angle. In this paper, $\mathbf{v}_R$ is set to zero. At R, the maximum Doppler frequency shift for the Iridium satellite in an orbit of 780 km is 40 kHz at the horizon and is given according to

$$f_{\text{Doppler}} = \frac{v_{\text{closing}} f}{c} \tag{43}$$

where v_{closing} is the relative velocity of T and R and is given as

$$v_{\text{closing}} = \hat{\mathbf{v}}_T \cdot \hat{\mathbf{k}} + \hat{\mathbf{v}}_R \cdot \hat{\mathbf{k}}. \tag{44}$$

DOI: 10.1002/sat

2.7. Satellite channel matrix

We may introduce signal transfer between T and R as proportional to the square root of power transfer through each subchannel [37]. In addition, a phase matrix is required that introduces the change in phase along a sub-channel as a result of path delay, Doppler shift and relative antenna offsets at both the receiver and transmitter.

An exponential phase component with phase angle, ϕ_{Ph}, is given by

$$\phi_{\text{Ph}} = 2\pi(f + f_{\text{Doppler}})\left(\frac{s+\zeta}{c}\right) + \psi_{\text{R}} + \psi_{\text{T}}. \tag{45}$$

In (45), f is the transmitted signal frequency, c is the speed of light, and $\psi_{\text{T,R}}$ represents a phase offset imposed at T and at R. For RHCP, we introduce a 90° retardation on the signal sent from $\hat{\mathbf{n}}$ with respect to $\hat{\mathbf{m}}$, while we introduce a 90° advance on $\hat{\mathbf{q}}$ with respect to $\hat{\mathbf{p}}$ and $\hat{\mathbf{r}}$. For the Orbcomm and GPS systems, a final 3×3 LoS channel matrix, from which we use the first two columns to calculate capacity resulting from *insitu* CP transmission from T, is given as [38, 39]

$$\mathbf{H} = \mathbf{X}_{\text{R}}^{\dagger}\bar{\mathbf{H}}\mathbf{X}_{\text{T}} \tag{46}$$

where the superscript denotes the Hermitian transpose. Mutual coupling matrices $\mathbf{X}_{\text{R}}$ and $\mathbf{X}_{\text{T}}$ introduce the isolation between polarizations into the channel matrix. A mutual coupling factor, ρ, of 0.3 [39], corresponding to an isolation coefficient of 10.45 dB is applied through mutual coupling matrices. This value is found to be where mutual coupling starts to degrade system performance, and we apply it universally as we assume no difference in isolation between any two ports. Values of 15 dB at R and 20 dB at T are given in [40], and so, we assume a worst case scenario. Mutual coupling matrices, including polarization $\hat{\mathbf{o}}$ at T, are given as

$$\mathbf{X}_{\text{R,T}} = \frac{1}{\sqrt{1+2\rho^2}}\begin{bmatrix} 1 & \rho & \rho \\ \rho & 1 & \rho \\ \rho & \rho & 1 \end{bmatrix}. \tag{47}$$

For an antenna with no isolation between polarizations, or unit values of ρ, the performance reverts to that of a singularly or uni-polarized antenna.

For the Iridium system, the channel matrix shall include a variable scattered NLoS component, $\tilde{\mathbf{H}}$, together with shadowing effects, and may be given as [38, 39]

$$\mathbf{H} = \mathbf{X}_{\text{R}}^{\dagger}\left(\sqrt{\frac{K}{1+K}}(\bar{\mathbf{H}} \odot \mathbf{S})\mathbf{X}_{\text{T}} + \sqrt{\frac{1}{1+K}}\tilde{\mathbf{H}}\right) \tag{48}$$

where $\odot$ represents the Hadamard, or elementwise, function, and $\mathbf{S}$ is a shadowing matrix.

3. RESULTS

We invoke the model used in [41] to provide analysis over antenna orientations at R within the FoV, according to orbital parameters. Faraday and path delay are calculated and included according to the work in [34]. Capacity for M orthogonal receivers and N orthogonal transmitters is given according to [42] as

$$C = \log_2\left|\left(\mathbf{I}_M + \frac{P_{\text{T}}}{P_{\text{N}}N}\mathbf{H}\mathbf{H}^{\dagger}\right)\right| \tag{49}$$

where P_{T} is the total transmit power at T, P_{N} is the noise power at R, $\mathbf{I}$ is an identity matrix, and $\mathbf{H}$ is the channel matrix. In this paper, unit transmit power is assumed for a satellite system analysis. The third orthogonal polarization at R provides a third degree of freedom and so provides an additional two

DOI: 10.1002/sat

link sub-channels to improve system performance. Simulations are performed over individual FoVs, using magnetic field and TEC data acquired during a random period. Each satellite begins an orbit at (0,0), where the orbit is calculated according to parameters laid out in Table I. The random orbit periods and FoV temporal positioning for each satellite are as follows:

- Iridium: 0000 UTC, November 17 to 0140 UTC November 17, with FoV data calculated every 10 min.
- Orbcomm: 0000 UTC, November 17 to 0140 UTC November 17, with FoV data calculated every 10 min.
- GPS: 0000 UTC, November 17 to 0000 UTC November 18, with FoV data calculated every hour.

Northern latitudes and eastern longitudes are deemed positive. The edge of the FoV is the point at which elevation at R is 0°and is orbit specific. In order to show the system improvement through implementation of a third orthogonal polarization at R, we introduce the notion of a percentage improvement in capacity of a 3×2 system over a 2×2 system. Figure 7 presents the capacity improvement resulting from the inclusion of a third orthogonal polarization at the receiver. In the case of the Iridium system, we are able to provide additional metrics to the analysis in the form of L-band local scattering effects

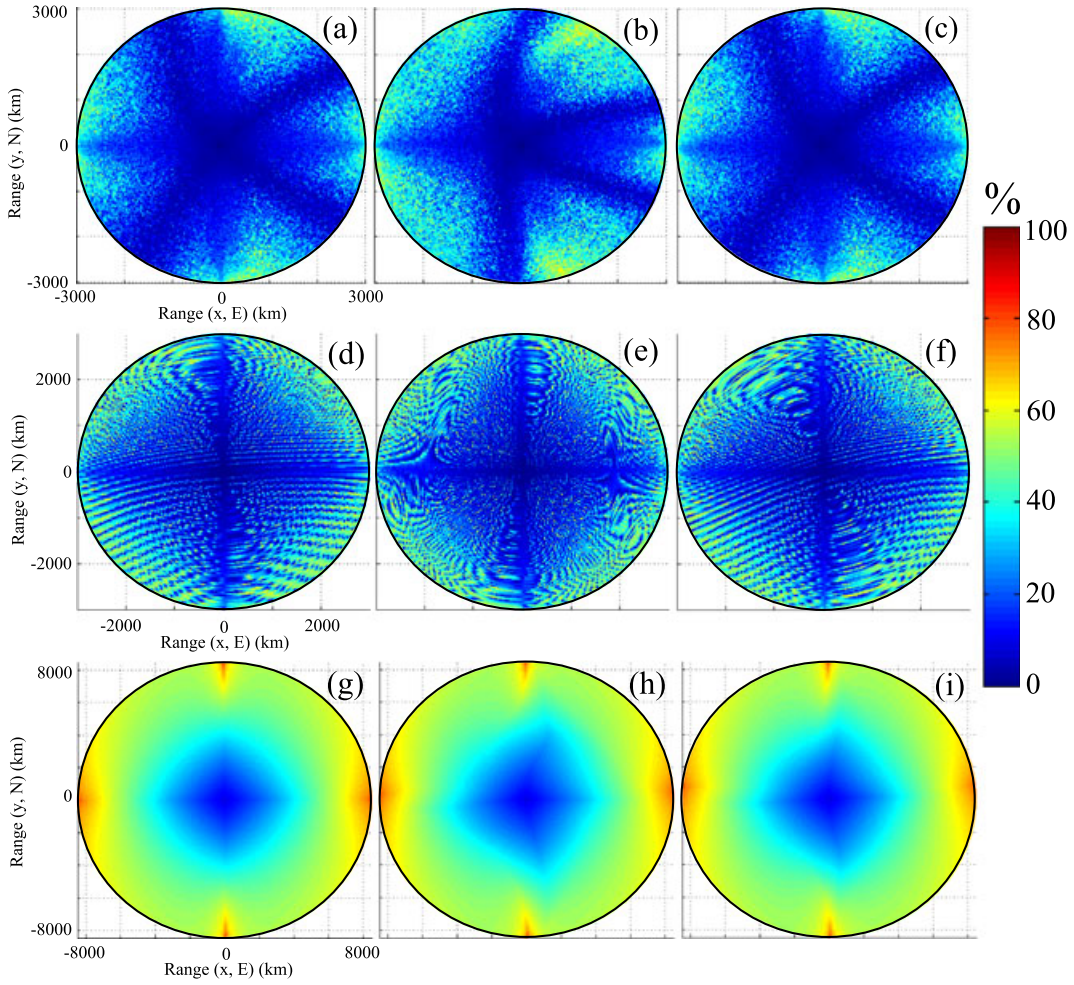

Figure 7. Simulated percentage improvement in system capacity over individual field-of-view, as a result of implementing a third orthogonal polarization at R. The following values in brackets are central positions on the ground of individual field-of-view. Rows: Iridium, L to R: (0°,0°), (0.7°,167.16°), (−1.41°,−25.09°); Orbcomm, L to R: (0°,0°), (0.39°,167.16°), (−0.78°,−25.68°); GPS, L to R: (0°,0°), (0.70°,−179.51°) (1.40°,0.98°). [Colour figure can be viewed at wileyonlinelibrary.com]

DOI: 10.1002/sat

in a LoS narrowband channel. Local scattering effects may further degrade receive performance due to multipath and synchronization issues [43]. A handheld receiver in an urban scenario is considered in our model, with local scattering effects included as a function of elevation. The data are given in Table XIII of [44]. We define the capacity improvement due to the inclusion of the third orthogonal polarization at the receiver as

$$D = \frac{C_{3\times2} - C_{2\times2}}{C_{2\times2}} \times 100. \tag{50}$$

For each of the satellite arrangements, the capacity improvement due to the inclusion of the third orthogonal polarization at R is shown by three large-FoVs in Figure 7 and is determined by orbit track parameters and the ionospheric effects of Faraday rotation and path delay. While it is to be expected that at the FoV center, or satellite nadir path, there is minimal if any improvement to capacity performance as a result of introducing a third orthogonal polarization at the receiver because it is parallel to the transmitter direction of propagation, it is of note that at no time does 3×2 capacity ever drop below that of the 2×2 system. This implies that capacity at the FoV center is not worsened by the addition of the third orthogonal polarization at R. A percentage capacity improvement is observed for all three satellite systems over each of the three global positions.

On average, and overall (L, l) positions analyzed over the orbital path, an increase in capacity performance as a result of the implementation of a third polarization $\hat{\mathbf{r}}$, orthogonal to the ground receiver patch antenna radiating surface, is observed for each satellite system. The average improvement, as a percentage of capacity performance compared with use of a conventional CP patch antenna at R, is given as follows:

- Iridium: $14.6 \pm 2.5\%$
- Orbcomm: $16.7 \pm 1.8\%$
- GPS: $38.8 \pm 3.1\%$.

At R, the patch antenna radiating surface is held orthogonal to the zenith position according to manufacturer's guidelines. This approach does not provide an idealized increase in system performance, but rather a consistent approach over the entire FoV. This may be considered as a proxy for the satellite position T being unknown at R. A beamsteering approach could subsequently be applied to enhance system performance through increasing gain in a link direction through phased antenna feeding techniques. As a consequence of applying a consistent approach to our analysis, the performance parameters do not take into account misalignment of the receive antenna with the zenith. At the FoV center, such misalignment would increase the capacity improvement because of the third orthogonal polarization $\hat{\mathbf{r}}$, as this polarization branch would mitigate any drop in performance on polarization branches $\hat{\mathbf{p}}$ and $\hat{\mathbf{q}}$, associated with a conventional CP patch antenna. The large improvement in average capacity performance over all (L, l) positions analyzed over the orbital path for the GPS system results from the increased misalignment of the antennas at T and R, because of a higher mid-Earth-orbit orbit. In effect, the maximum antenna misalignment experienced by each system due to the arrangement described in Section 2.2 may be given by (5) and is as follows:

- Iridium: 27°
- Orbcomm: 26.9°
- GPS: 76.1°.

The increase in diversity gain [45] over the orbital path due to the inclusion of the third orthogonal polarization at R is calculated for each satellite system and is shown in Figure 8. We assume the patch antenna radiating surface is once again held orthogonal to the zenith position. Applying maximal ratio combining at R, the increase in diversity gain for 99% communication reliability is given as follows:

- Iridium: 2.43 dB
- Orbcomm: 2.23 dB
- GPS: 3.18 dB.

DOI: 10.1002/sat

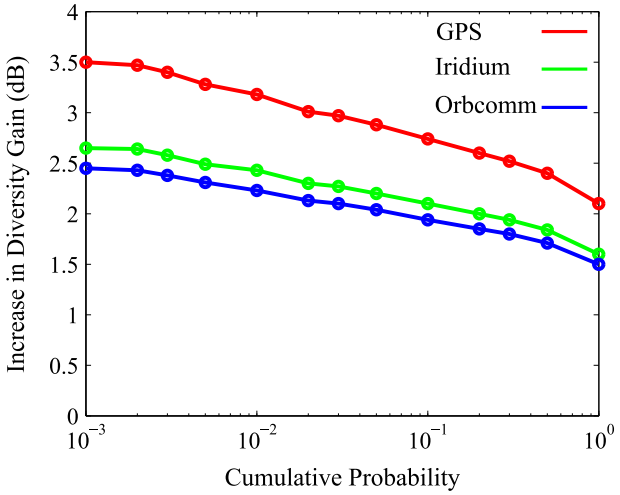

Figure 8. Simulated increase in diversity gain (dB) over an orbital path for each satellite, as a result of implementing a third orthogonal polarization at R. [Colour figure can be viewed at wileyonlinelibrary.com]

4. CONCLUSION

This paper provides model analysis which, through a fundamental physical design approach, suggests that the inclusion of a third polarization at a ground receiver, orthogonal to an existing patch or helical structure, provides over a large non-geosynchronous satellite FoV the following advantages:

- increased capacity over a majority of a FoV, or antenna orientations
- provision of orientation robustness in instances of antenna misalignment
- increased FoV range extending the outer edge of the FoV
- increased diversity gain over the orbit path, providing communication reliability with a reduction in transmit power at the satellite
- implementable on ground receiver, requiring no intervention at the satellite.

This is particularly relevant to LEO satellite systems, where link geometry changes rapidly, and near horizontal link geometry occurs frequently. A tri-orthogonal approach at the ground receiver renders a satellite link less dependent on alignment, as at least two orthogonal receive polarizations are offered at the receiver for any receive link direction.

For a conventional CP receive antenna, a CP signal is only able to be received where perfect transmitter-receiver antenna alignment exists, typically when a satellite is near the zenith position of the ground receive patch antenna, due to design constraints and manufacturer guidelines. Signal polarization becomes EP as receive link geometry deviates from perfect transmitter-receiver antenna alignment, ultimately resulting in horizontally polarized signal reception at the receiver horizon. Coupled with a reduced receive antenna gain at lower elevation angles, this impairs cross-polarization rejection and reduces system capacity. The ability to maintain gain at lower elevation angles, while maintaining polarization diversity, would increase link range and extend the FoV.

We have considered the case whereby the ground receiver patch antenna radiating surface is orthogonal to the zenith position. This alignment is unlikely to be maintained for most applications, because of local topography and movement. At or near the FoV center, this suggests that, where a low or negligible improvement in capacity due to a third orthogonal polarization branch is observed in our simulations, the probability of a capacity improvement as observed in the outer FoV edges of our simulations is increased. This would additionally increase the diversity gain of the satellite system.

The inclusion of a third polarization at the ground receiver, orthogonal to the radiating surface of the antenna and so orthogonal to conventional patch antenna polarizations, provides additional polarization diversity. Through no alteration to the satellite transmission mechanism, such an arrangement provides a capacity improvement and additional diversity gain over a FoV for three distinct satellites. Real-time global ionospheric data and physical satellite characteristics are used to provide these results. The capacity improvement and additional diversity gain are a consequence of increased gain at low-elevation angles, coupled with enhanced polarization diversity performance at low-elevation angles.

DOI: 10.1002/sat

REFERENCES

1. Pozar D. *Microwave Engineering* (4th edn). John Wiley and Sons: Hoboken, United States, 2011.
2. Cobham Plc. *GPS antenna installation guidelines*. (Available from: https://www.cobham.com/media/5048/gpsantennainstallationguide.pdf), [accessed on 2015].
3. Taoglas Ltd. *GPS patch integration application note*. (Available from: http://www.taoglas.com/images/product_images/original_images/TAOGLAS%20-%20GPS%20Patch%20Antenna%20Integration%20Application%20Note%28APN-12-8-002.B%29.pdf), [accessed on 2015].
4. Antcom Corporation. Combined Inmarsat/Iridium/GPS Thuraya antennas for ground and airborne applications. *Technical Report*. (Available from: http://www.antcom.com/documents/catalogs/CombinedL-Band_Inmarsat_Thuraya_IridiumandGPSAntennas.pdf), [accessed on 2016].
5. Pozar DM, Schaubert D. *Microstrip Antennas: The Analysis And Design Of Microstrip Antennas And Arrays*, Electrical Engineering, Antennas And Propagation. Wiley: New Delhi, India, 1995. (Available from: https://books.google.co.uk/books?id=3MJ7UmQMaOIC).
6. Maus S, Macmillan S, McLean S, Hamilton B, Thomson A, Nair M, Rollins C. The US/UK world magnetic model 2010–2015, *NOAA technical report NESDIS/NGDC*: NOAA, Boulder, CO,USA, 2010. (Available from: http://www.ngdc.noaa.gov/geomag/WMM/data/WMM2010/WMM2010_Report.pdf) [accessed on 2014].
7. Ilčev SD. *Global Mobile Satellite Communications: For Maritime, Land And Aeronautical Applications.* Springer: Dordrecht, Netherlands, 2005. (Available from: https://books.google.co.uk/books?id=b2KyCT1AnO4C).
8. Toh BY, Cahill R, Fusco VF. Understanding and measuring circular polarization. *IEEE Transactions on Education* 2003; **46**(3):313–318.
9. Tirró S. *Satellite Communication Systems Design.* Springer: US, 1993. (Available from: https://books.google.co.uk/books?id=AdwFdgykaMUC).
10. Roddy D. *Satellite Communications, Fourth Edition (Professional Engineering).* McGraw-Hill Professional: New York, NY, United States, 2006.
11. Farserotu J, Prasad R. A survey of future broadband multimedia satellite systems, issues and trends. *IEEE Communications Magazine* 2000; **38**(6):128–133. (Available from: http://dx.doi.org/10.1109/35.846084) [accessed on 2014].
12. Panther G. Patch antennas for the new GNSS, *GPS World*. (Available from: http://gpsworld.com/wirelesspatch-antennas-new-gnss-12552/http://gpsworld.com/wirelesspatch-antennas-new-gnss-12552/), [accessed on 2015].
13. Wright P, Quegan S, Wheadon N, Hall C. Faraday rotation effects on L-band spaceborne SAR data. *IEEE Transactions on Geoscience and Remote Sensing* 2003; **41**(12):2735–2744.
14. Padros N, Ortigosa JI, Baker J, Iskander MF, Thornberg B. Comparative study of high-performance GPS receiving antenna designs. *IEEE Transactions on Antennas and Propagation* 1997; **45**(4):698–706.
15. Andrews M, Mitra P, de Carvalho R. Tripling the capacity of wireless communications using electromagnetic polarization. *Nature* 2001; **409**:316–318.
16. Horvath P, Frigyes I. Application of the 3D polarization concept in satellite MIMO systems, *Proc. IEEE Global Communications Conference (GlobeCom)*: San Francisco, USA, 2006. (Available from: dx.doi.org/10.1109/GLOCOM.2006.481) [accessed on 2013].
17. Iridium Communications Inc. *Iridium Global Network*. (Available from: http://www.iridium.com//network/globalnetwork) [accessed on 2014].
18. Johannsen K. Mobile P-service satellite system comparison. *International Journal of Satellite Communications* 1995; **13**:453–471. (Available from: http://onlinelibrary.wiley.com/doi/10.1002/sat.4600130604/pdf) [accessed on 2014].
19. Coverdale DR. Potential applications of the Orbcomm global messaging system to US military operations, *Naval Postgraduate School, Monterey, California* 1995. (Available from: http://https://core.ac.uk/download/pdf/36724187.pdf) [accessed on 2013].
20. Orbcomm Inc. *Networks*. (Available from: http://www.orbcomm.com/networks), [accessed on 2014].
21. United States Government. GPS. GOV. (Available from: http://www.gps.gov), [accessed on 2015].
22. Movable Type Ltd. *Calculate distance, bearing and more between latitude/longitude points*. (Available from: http://www.movable-type.co.uk/scripts/latlong.html), [accessed on 2014].
23. Arapoglou P, Zamkotsian M, Cottis P. Dual polarization MIMO in LMS broadcasting systems: possible benefits and challenges. *International Journal of Satellite Communications,* 2011; **29**:349–366.
24. Liolis K, Gomez-Vilardebo J, Casini E, Perez-Neira A. Statistical modeling of dual-polarized MIMO land mobile satellite channels. *IEEE Transactions on Communications* 2010November; **58**(11):3077–3083. (Available from: http://dx.doi.org/10.1109/TCOMM.2010.091710.090507) Published in 2010. [accessed on 2014].
25. Orfanidis S. *Electromagnetic Waves And Antennas Book.* Rutgers University: NJ, 2002. (Available from: http://www.ece.rutgers.edu/faculty/orfanidis) [accessed on 2014].
26. Orbcomm LLC. *Orbcomm system overview A80TD0008 - revision G*. (Available from: http://www.m2mconnectivity.com.au/sites/default/files/more-information/System_Overview_Rev_G.pdf), [accessed on 2014].
27. Schuss JJ, Carlson T, Francois R, Maloney P, Rohwer A, Upton J, Wardle L, Smith R. Design of the Iridium phased array antennas. *In IEEE Antennas and Propagation Society International Symposium, 1993*, Vol. 1: Ann Arbor, MI, USA, 1993; 218–221.
28. Marquis WA, Reigh DL. The GPS block IIR and IIR-M broadcast L-band antenna panel: its pattern and performance. *Navigation* 2015; **62**(4):329–347. (Available from: http://dx.doi.org/10.1002/navi.123) [accessed on 2016].
29. Antenna Research Associates. *Orbcomm antennas*. (Available from: http://www.ic72.com/pdf_file/a/187619.pdf), [accessed on 2016].
30. Inevitable Technologies. *Orbcomm antennas*. (Available from: http://www.inevtech.com/orbcomm-antennas), [accessed on 2016].
31. Hall P. Application of sequential feeding to wide bandwidth, circularly polarised microstrip patch arrays. *IEE Proceedings H Microwaves, Antennas and Propagation* 1989; **136**(5):390–398.
32. International Telecommunications Union (ITU-R). Ionospheric propagation data and prediction methods required for the design of satellite services and systems, 2013, 531–539.

DOI: 10.1002/sat

33. National Oceanic, Atmospheric Administration. *Coupled thermosphere ionosphere plasmasphere electrodynamics model*. (Available from: http://helios.swpc.noaa.gov/ctipe/about.html), [accessed on 2014].
34. Lawrence N, Hansen H, Abbott D. 3-D low earth orbit vector estimation of Faraday rotation and path delay. *IEEE Access* 2015; **3**:1684–1694.
35. Jehle M, Ruegg M, Small D, Meier E, Nuesch D. Estimation of ionospheric TEC and Faraday rotation for L-band SAR. *Proc. SPIE*, Vol. 5979, 2005; 252–260.
36. Jehle M, Ruegg M, Zuberbuhler L, Small D, Meier E. Measurement of ionospheric Faraday rotation in simulated and real spaceborne SAR data. *IEEE Transactions on Geoscience and Remote Sensing* 2009; **47**(5):1512–1523. (Available from: http://dx.doi.org/10.1109/TGRS.2008.2004710) [accessed on 2013].
37. Lawrence N, Davis LM, Haley D. A polarimetric line-of-sight channel model for MIMO satellite communications. *In IEEE Proc. 2013 Communications Theory Workshop (AusCTW), Australia*: Adelaide, SA, Australia, 2013; 99–104.
38. Arapoglou P, Liolis K, Bertinelli M, Panagopoulos A, Cottis P, De Gaudenzi R. MIMO over satellite: a review. *IEEE Communications Surveys Tutorials* 2011; **13**(1):27–51. (Available from: http://dx.doi.org/10.1109/SURV.2011.033110.00072) [accessed on 2013].
39. Sirianunpiboon S, Howard S, Calderbank A, Davis L. Fully-polarimetric MIMO to improve throughput and reliability across propagation conditions. *In IEEE 70th Vehicular Technology Conference Fall (VTC 2009-Fall)*, 2009; 1–5. (Available from: http://dx.doi.org/10.1109/VETECF.2009.5379016) [accessed on 2013].
40. King PR, Stavrou S. Low elevation wideband land mobile satellite MIMO channel characteristics. *IEEE Transactions on Wireless Communications* 2007; **6**(7):2712–2720.
41. Lawrence NP, Ng BWH, Hansen HJ, Abbott D. Analysis of millimetre-wave polarization diverse multiple-input multiple-output capacity. *Royal Society Open Science* 2015; **2**(12). (Available from: http://rsos.royalsocietypublishing.org/content/2/12/150322).
42. Bohagen F, Orten P, Oien GE. Construction and capacity analysis of high-rank line-of-sight MIMO channels. *IEEE Wireless Communications and Networking Conference*, Vol. 1: New Orleans, USA, 2005; 432–437. (Available from: http://dx.doi.org/10.1109/WCNC.2005.1424539) [accessed on 2013].
43. Kos T, Markezic I, Pokrajcic J. Effects of multipath reception on GPS positioning performance. *Proc. 2010 IEEE ELMAR*: IEEE: Zadar, Croatia, 2010; 399–402.
44. Fontan FP, Vazquez-Castro M, Cabado CE, Garcia JP, Kubista E. Statistical modeling of the LMS channel. *IEEE Transactions on Vehicular Technology* 2001Nov; **50**(6):1549–1567.
45. Adve R. *Receive Diversity*, 2008. (Available from: http://www.comm.toronto.edu/~rsadve/Notes/DiversityReceive.pdf) [accessed on 2013].

APPENDIX

Table A1. List of variables.

Reference	Description
T	Transmitter (satellite)
R	Receiver (ground)
r_{plot}	Ground range
r_{e}	Earth radius
s	Propagation distance
d	Orbit Height
u	$r_{\text{e}} + d$
α	Off-nadir angle
γ	Earth centered arc angle
κ	90°-elevation at R
θ_{T}	Azimuthal angle, +ve a/cw from east
L	Latitude
l	Longitude
L_{u}	User specified latitude
l_{u}	User specified longitude
h	Height (m)
L_{o}	Original FoV center latitude
l_{o}	Original FoV center longitude
L_{c}	Calculated FoV center latitude
l_{c}	Calculated FoV center longitude
$\mathbf{b}$	Terrestrial magnetic vector
ψ_{FR}	Faraday Rotation (rads)
$\mathbf{K}_{\text{ref}}$	Ionospheric refraction constant
e	Electronic charge (C)
m	Electron mass (kg)
ϵ_0	Permittivity of free space (Fm^{-1})
TEC	Total electron content

DOI: 10.1002/sat

Table A1. *Continued.*

Reference	Description
ζ	Path delay (m)
i,k_{FR}	Loop increments for calculation of Faraday rotation
δ	Magnetic field declination
ι	Magnetic field inclination
θ_{inc}	Orbital inclination angle
θ_{bFoV}	Bearing angle at FoV center to next FoV center
θ_b	Bearing angle at FoV center to (L, l) position in FoV
θ_{sb}	Shortest route bearing angle
$\hat{\mathbf{k}}$	Propagation unit vector
$\hat{\mathbf{m}}$	Unit vector aligned in easterly direction at T
$\hat{\mathbf{n}}$	Unit vector aligned in northerly direction at T
$\hat{\mathbf{p}}$	Unit vector aligned in easterly direction at R
$\hat{\mathbf{q}}$	Unit vector aligned in northerly direction at R
$\hat{\mathbf{r}}$	Unit vector aligned in Earth centered radial direction at R
t	Time (secs)
ϕ	Angle made with dipole (rads)
$\mathbf{Y}$	Set of received signals at R
$\mathbf{X}$	Set of transmitted signals at T
$\mathbf{H}$	Channel matrix
$\mathbf{N}$	Set of noise signals at R
f	Frequency (Hz)
c	Speed of light in vacuo (ms^{-1})
ϕ_{Ph}	Phase change over channel (rads)
$\Phi_{T,R}$	Phase offset at T,R
K	Ricean K-factor
$\mathbf{X}_{T,R}$	Mutual coupling matrix
ρ	Mutual coupling coefficient
P	Power (W)
G	Gain (dB)
$\hat{\mathbf{v}}$	Generic unit vector for polarization mismatch
λ	Wavelength (m)
e_{pol}	Polarization mismatch (dB)
L_{atmos}	Atmospheric attenuation (dB)
n_e	Electron density (m^{-3})
$f_{Doppler}$	Doppler frequency shift (Hz)
$v_{closing}$	Relative velocity of T and R (ms^{-1})
$\mathbf{v}_{T,R}$	Vector describing motion at T,R
C	Capacity (bits/s/Hz)
D	Percentage improvement in capacity (%)

AUTHORS' BIOGRAPHIES

Nicholas P. Lawrence was born in Chichester, UK, in 1972. He received the BSc (Hons) degree, 1995, in physics from the University of Leicester, UK, and the MSc degree with distinction, 1997, in microwave solid state physics from the University of Portsmouth, UK. He received the MPhil degree in, 2002, in fibre optic sensing techniques from the University of Southampton, UK. He has since worked as a radio frequency power amplifier engineer specialising in linearity techniques employed in applications ranging from high power military applications to commercial COFDM broadcast systems. He is a Chartered Engineer with the Institute of Engineering and Technology (IET), UK, since 2004. He is currently working towards his PhD at the University of Adelaide, Australia, under Hedley Hansen and Derek Abbott, where his work focuses on applications of MIMO polarimetry in remote sensing and communication.

DOI: 10.1002/sat

Hedley J. Hansen (M'98) was born in Port Elizabeth, South Africa, in 1957. He received the BSc (Hons), MSc (*cum laude*) and PhD degrees from the University of Natal, Durban, South Africa, in 1980, 1983 and 1988, respectively. His PhD research, under Malcolm W. J. Scourfield, was concerned with magnetospheric wave particle interaction processes that give rise to the optical aurora. In 1988, he joined the Space Plasma Waves Group at the University of Newcastle, NSW, as a Postdoctoral Research Associate. The group maintained arrays of induction magnetometers in Australian Antarctic Territory and across the Australian Mainland. He moved to the RF Technology Group, Electronic Warfare and Radar Division, Defence Science and Technology Organisation, Edinburgh, South Australia, in 1996 as a Senior Research Scientist. His professional interests lie in RF remote sensing at millimetre and submillimetre wavelengths, in microstrip antenna design and in phased array and miniaturized radar technologies. He is an adjunct senior lecturer at the University of Adelaide, and he currently chairs the AP&MTT Chapter (South Australian section) of the IEEE. Dr. Hansen is a member of both the American Geophysical Union (AGU) and the Australian Institute of Physics (AIP).

Derek Abbott (M'85–SM'99–F'05) was born in South Kensington, London, UK, in 1960. He received the BSc (Hons.) degree in physics from Loughborough University, UK, in 1982, and the PhD degree in electrical and electronic engineering from the University of Adelaide, Australia, in 1995, under K. Eshraghian and B. R. Davis. From 1978 to 1986, he was a Research Engineer with the GEC Hirst Research Centre, London. From 1986 to 1987, he was a VLSI Design Engineer with Austek Microsystems, Australia. Since 1987, he has been with the University of Adelaide, where he is currently a full professor with the School of Electrical and Electronic Engineering. He holds over 800 publications and has been an invited speaker at over 100 institutions. He is a fellow of the Institute of Physics (IOP). He has received a number of awards, including the South Australian Tall Poppy Award for Science in 2004, the Premier's SA Great Award in Science and Technology for outstanding contributions to South Australia in 2004 and the Australian Research Council Future Fellowship in 2012. He has served as an Editor and/or Guest Editor for a number of journals, including the IEEE JOURNAL OF SOLID-STATE CIRCUITS, the *Journal of Optics B* (IOP), *Microelectronics Journal* (Elsevier), *Chaos* (AIP), *Smart Structures and Materials* (IOP), *Fluctuation Noise Letters* (World Scientific), *PLOSONE*, PROCEEDINGS OF THE IEEE and IEEE PHOTONICS JOURNAL. He is currently on the editorial boards of Nature's *Scientific Reports*, IEEE ACCESS and *Royal Society Open Science* (RSOS). He has co-edited *Quantum Aspects of Life*, Imperial College Press, co-authored *Stochastic Resonance* (Cambridge University Press) and *Terahertz Imaging for Biomedical Applications* (Springer-Verlag). Professor Abbott is a Fellow of the IEEE and his interests are in the area of multidisciplinary physics and electronic engineering applied to complex systems.

DOI: 10.1002/sat